Acid−Base Controllable Molecular Shuttles†

Peter R. Ashton,‡ Roberto Ballardini,§ Vincenzo Balzani,*,# Ian Baxter,⊥ Alberto Credi,# Matthew C. T. Fyfe,‡ Maria Teresa Gandolfi,# Marcos Gómez-López,‡ M.-Victoria Martínez-Díaz,‡ Arianna Piersanti,‡ Neil Spencer,‡ J. Fraser Stoddart,*,‡,¶ Margherita Venturi,# Andrew J. P. White,⊥ and David J. Williams*,⊥

Contribution from The School of Chemistry, The University of Birmingham, Edgbaston, Birmingham B15 2TT, UK, Istituto FRAE-CNR, via Gobetti 101, 40129, Bologna, Italy, Dipartimento di Chimica "G. Ciamician" dell'Università di Bologna, via Selmi 2, 40126, Bologna, Italy, and The Department of Chemistry, Imperial College, South Kensington, London SW7 2AY, UK

Received June 22, 1998

Abstract: Two novel [2]rotaxanes, comprised of a dibenzo[24]crown-8 (DB24C8) macroring bound mechanically to a chemical "dumbbell" possessing two different recognition sites—viz., secondary dialkylammonium (NH_2^+) and 4,4′-bipyridinium ($Bpym^{2+}$) units—have been synthesized by using the supramolecular assistance to synthesis provided by, inter alia, hydrogen bonding interactions. One of these rotaxanes bears a fluorescent and redox-active anthracene (Anth) stopper unit. NMR spectroscopy and X-ray crystallography have demonstrated that the DB24C8 macroring exhibits complete selectivity for the NH_2^+ recognition sites, i.e., that the [2]rotaxanes exist as only one of two possible translational isomers. Deprotonation of the rotaxanes' NH_2^+ centers effects a quantitative displacement of the DB24C8 macroring to the $Bpym^{2+}$ recognition site, an outcome that can be reversed by acid treatment. The switching processes have been investigated by ^1H NMR spectroscopy and, for the Anth-bearing rotaxane, by electrochemical and photophysical measurements. Furthermore, it is possible to drive the DB24C8 macroring from the dumbbell's $Bpym^{2+}$ unit, in the deprotonated form of the Anth-bearing rotaxane, by destroying the stabilizing DB24C8−$Bpym^{2+}$ charge-transfer interactions via electrochemical reduction. The photochemical and photophysical properties of this rotaxane (in both its protonated and deprotonated states) have also been investigated.

Introduction

Molecular information processing, which exploits the switching of molecular and supramolecular systems between clearly identifiable states, is a topic of rapidly increasing interest.[1] Aside from the continuing attention being paid to photochemically active and electrochromic compounds,[2,3] along with chemical sensors,[4] much focus is being centered on molecular and supramolecular systems in which the relative positions of their component parts can be altered by an external stimulus. Appealing examples of chemical species that have mechanically movable component parts are suitably designed catenanes, rotaxanes, and pseudorotaxanes.[5] The relative displacements of these parts can be induced by chemical[6] or electrical[7] energies, as well as by light,[8] and can be monitored by a variety of techniques, such as NMR, absorption and emission spectroscopies, along with electrochemistry.

Rotaxanes are fashioned from dumbbell-shaped and macrocyclic components that are bound to one another mechanically. In the past few years, a large number of these molecular species, based on bipyridinium-type ($Bpym^{2+}$) π-electron deficient and aromatic π-electron rich units, have been synthesized, using the supramolecular assistance to synthesis provided by a variety of

† Molecular Meccano, Part 46. For Part 45, see: Bravo, J. A.; Raymo, F. M.; Stoddart, J. F.; White, A. J. P.; Williams, D. J. *Eur. J. Org. Chem.* **1998**, 2565−2571.

‡ University of Birmingham.

§ Istituto FRAE-CNR.

Università di Bologna.

⊥ Imperial College.

¶ Current address: Department of Chemistry and Biochemistry, University of California, Los Angeles, CA 90095.

(1) (a) *Molecular Electronic Devices*; Carter, F. L., Siatkowsky, R. E., Woltjien, H., Eds.; Elsevier: Amsterdam, 1988. (b) Kuhn, H. In *Molecular Electronics*; Lazarev, P. I., Ed.; Kluwer: Dordrecht, 1991; Chapter 12. (c) Lehn, J.-M. *Supramolecular Chemistry—Concepts and Perspectives*; VCH: Weinheim, 1995. (d) Verdaguer, M. *Science* **1996**, *272*, 698−699. (e) Goldhaber-Gordon, D.; Montemerlo, M. S.; Love, J. C.; Opiteck, G. J.; Ellenbogen, J. C. *Proc. IEEE* **1997**, *85*, 521−540. (f) Astruc, D. *Acc. Chem. Res.* **1997**, *30*, 383−391.

(2) For reviews, see: (a) *Photochromism—Molecules and Systems*; Dürr, H., Bouas-Laurent, H., Eds.; Elsevier: Amsterdam, 1990. (b) Feringa, L. B.; Jager, W. F.; de Lange, B. *Tetrahedron* **1993**, *49*, 8267−8310. (c) Balzani, V.; Scandola, F. In *Comprehensive Supramolecular Chemistry*; Reinhoudt, D. N., Ed.; Pergamon: Oxford, 1996; Vol. 10, pp 687−746.

(3) (a) Kawai, S. H.; Gilat, S. L.; Posinet, R.; Lehn, J.-M. *Chem. Eur. J.* **1995**, *1*, 285−293. (b) Matsushima, R.; Mizuno, H.; Itoh, H. *Photochem. Photobiol. A Chem.* **1995**, *89*, 251−256. (c) Tsivgoulis, G. M.; Lehn, J.-M. *Chem. Eur. J.* **1996**, *2*, 1399−1406. (d) Pina, F.; Melo, M. J.; Maestri, M.; Ballardini, R.; Balzani, V. *J. Am. Chem. Soc.* **1997**, *119*, 5556−5561. (e) Kollmannsberger, M.; Gareis, T.; Heinl, S.; Breu, J.; Daub. J. *Angew. Chem., Int. Ed. Engl.* **1997**, *36*, 1333−1335. (f) Asakawa, M.; Ashton, P. R.; Balzani, V.; Credi, A.; Mattersteig, G.; Matthews, O. A.; Montalti, M.; Spencer, N.; Stoddart, J. F.; Venturi, M. *Chem. Eur. J.* **1997**, *3*, 1992−1996.

(4) (a) *Fluorescent Chemosensors for Ion and Molecule Recognition*; ACS Symp. Ser. No. 538; Czarnik, A. W., Ed.; American Chemical Society: Washington, DC, 1992. (b) de Silva, A. P.; Gunaratne, H. Q. N.; Gunnlaugsson, T.; Huxley, A. J. M.; McCoy, C. P.; Rademacher, J. T.; Rice, T. E. *Chem. Rev.* **1997**, *97*, 1515−1566.

(5) (a) Benniston, A. C. *Chem. Soc. Rev.* **1996**, *25*, 427−435. (b) Balzani, V.; Gómez-López, M.; Stoddart, J. F. *Acc. Chem. Res.* **1998**, *31*, 405−414. (c) Sauvage, J.-P. *Acc. Chem. Res.* **1998**, *31*, 611−619.

(6) Recent prominent articles: (a) Bissell, R. A.; Córdova, E.; Kaifer, A. E.; Stoddart, J. F. *Nature* **1994**, *369*, 133−137. (b) Amabilino, D. B.; Dietrich-Buchecker, C. O.; Livoreil, A.; Pérez-García, L.; Sauvage, J.-P.; Stoddart, J. F. *J. Am. Chem. Soc.* **1996**, *118*, 3905−3913. (c) Credi, A.; Balzani, V.; Langford, S. J.; Stoddart, J. F. *J. Am. Chem. Soc.* **1997**, *119*, 2679−2681.

10.1021/ja982167m CCC: $15.00
Published on Web 11/10/1998

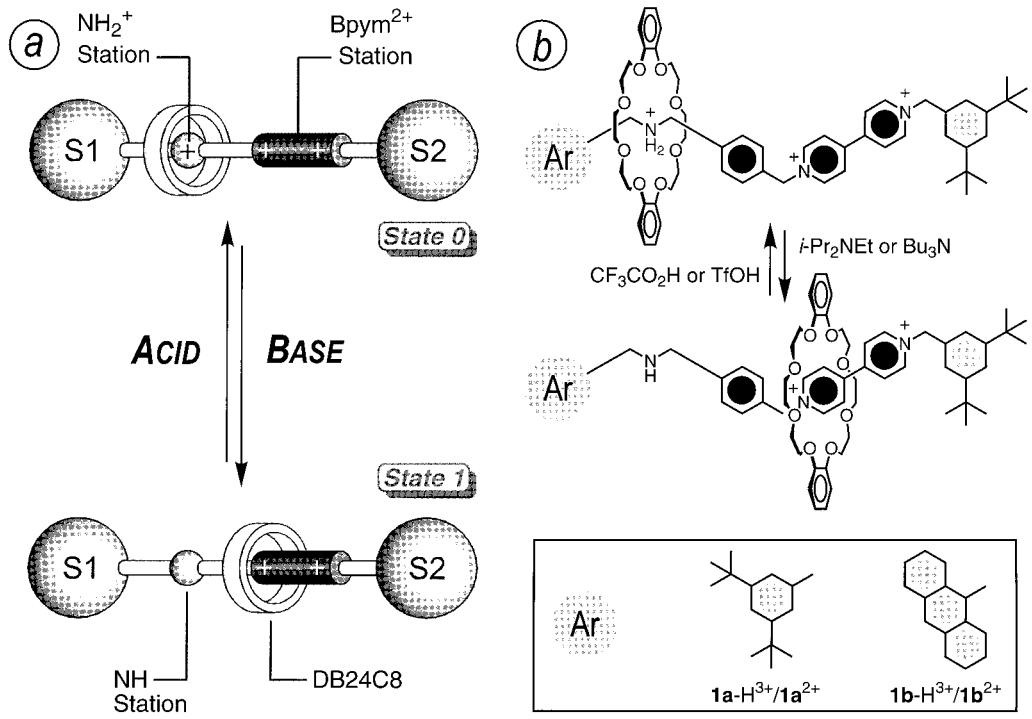

Figure 1. (a) Cartoon showing an acid−base controllable molecular shuttle. Initially (***State 0***), the macrocyclic component resides solely on the NH_2^+ station. After treatment with a nonnucleophilic base, deprotonation coerces the macroring to move to the $Bpym^{2+}$ station (***State 1***). Addition of acid regenerates the NH_2^+ center, moving the macrocyclic component back to bind its original station and rendering the switching cycle reversible. (b) Structural formulas of the switchable [2]rotaxanes described here.

noncovalent interactions.[9] More recently, the formation of pseudorotaxane inclusion complexes between secondary dialkylammonium ions (e.g., the dibenzylammonium ion (DBA^+)) and macrocyclic polyethers (e.g., dibenzo[24]crown-8 (DB24C8) and bis-*p*-phenylene[34]crown-10 (BPP34C10)) as a result of, inter alia, [N$^+$−H···O] and [C−H···O] hydrogen bonds has been reported.[10,11] Here, we describe[12] the novel switchable [2]-rotaxanes **1a**-H^{3+} and **1b**-H^{3+} (Figure 1), based upon a dumbbell-shaped component—possessing both secondary dialkylammonium (NH_2^+) and $Bpym^{2+}$ units, i.e., two different recognition sites—that is threaded through the DB24C8 macroring. In rotaxanes of this type, it is possible to switch the macroring's position between the two different recognition sites by the action of external stimuli. In [2]rotaxane **1b**-H^{3+}, we have used an anthracene (Anth) moiety as a stopper, as we thought that its absorption, luminescence, and redox properties would be useful for (1) monitoring the system's state and (2) propelling the macroring by photochemical and electrochemical stimulation.

For both **1a**-H^{3+} and **1b**-H^{3+}, the DB24C8 macroring should exhibit complete selectivity for the NH_2^+ recognition site so that the [2]rotaxanes exist as only one of two possible translational isomers. Deprotonation of the NH_2^+ center can be expected to induce the displacement of the macroring to the $Bpym^{2+}$ station, a displacement that should be reversed (Figure 1) upon reprotonation. These switching processes have been investigated, for both **1a**-H^{3+} and **1b**-H^{3+}, by ^{1}H NMR spectroscopy and, in the case of **1b**-H^{3+}, by electrochemical and photophysical measurements. We also conjectured that it should be possible to displace the crown ether from the $Bpym^{2+}$ station by destroying the catechol-$Bpym^{2+}$ charge transfer (CT) interactions in the deprotonated [2]rotaxanes **1a**$^{2+}$ and **1b**$^{2+}$ through either electrochemical (1) reduction of the $Bpym^{2+}$ station or (2) oxidation of the DB24C8 macroring. The photochemical and photophysical properties of **1b**$^{2+}$ have also been studied because of the presence of the potentially photoreactive and fluorescent Anth unit.

Results and Discussion

Synthesis.[13] Since DB24C8 shows[14] very little binding affinity toward $Bpym^{2+}$ dications and is able[10] to form pseu-

(7) For recent leading papers, see refs 3f, 6a, and the following: (a) Livoreil, A.; Dietrich-Buchecker, C. O.; Sauvage, J.-P. *J. Am. Chem. Soc.* **1994**, *116*, 9399−9400. (b) Ashton, P. R.; Ballardini, R.; Balzani, V.; Credi, A.; Gandolfi, M. T.; Menzer, S.; Pérez-García, L.; Prodi, L.; Stoddart, J. F.; Venturi, M.; White, A. J. P.; Williams, D. J. *J. Am. Chem. Soc.* **1995**, *117*, 11171−11197. (c) Ashton, P. R.; Ballardini, R.; Balzani, V.; Boyd, S. E.; Credi, A.; Gandolfi, M. T.; Gómez-López, M.; Iqbal, S.; Philp, D.; Preece, J. A.; Prodi, L.; Ricketts, H. G.; Stoddart, J. F.; Tolley, M. S.; Venturi, M.; White, A. J. P.; Williams, D. J. *Chem Eur. J.* **1997**, *3*, 152−170. (d) Livoreil, A.; Sauvage, J.-P.; Armaroli, N.; Balzani, V.; Flamigni, L.; Ventura, B. *J. Am. Chem. Soc.* **1997**, *119*, 12114−12124. (e) Asakawa, M.; Ashton, P. R.; Balzani, V.; Credi, A.; Hamers, C.; Mattersteig, G.; Montalti, M.; Shipway, A. N.; Spencer, N.; Stoddart, J. F.; Tolley, M. S.; Venturi, M.; White, A. J. P.; Williams, D. J. *Angew. Chem., Int. Ed.* **1998**, *37*, 333−337.

(8) For recent leading papers, see refs 7c, 7d, and the following: (a) Bauer, M.; Müller, W. M.; Müller, U.; Rissanen, K.; Vögtle, F. *Liebigs Ann.* **1995**, 649−656. (b) Benniston, A. C.; Harriman, A.; Lynch, V. M. *J. Am. Chem. Soc.* **1995**, *117*, 5275−5291.

(9) (a) Amabilino, D. B.; Stoddart, J. F. *Chem. Rev.* **1995**, *95*, 2725−2828. (b) Philp, D.; Stoddart, J. F. *Angew. Chem., Int. Ed. Engl.* **1996**, *35*, 1154−1196.

(10) (a) Kolchinski, A. G.; Busch, D. H.; Alcock, N. W. *J. Chem. Soc., Chem. Commun.* **1995**, 1289−1291. (b) Ashton, P. R.; Chrystal, E. J. T.; Glink, P. T.; Menzer, S.; Schiavo, C.; Spencer, N.; Stoddart, J. F.; Tasker, P. A.; White, A. J. P.; Williams, D. J. *Chem. Eur. J.* **1996**, *2*, 709−728. (c) Montalti, M.; Ballardini, R.; Prodi, L.; Balzani, V. *Chem. Commun.* **1996**, 2011−2012. (d) Ashton, P. R.; Ballardini, R.; Balzani, V.; Gómez-López, M.; Lawrence, S. E.; Martínez-Díaz, M.-V.; Montalti, M.; Piersanti, A.; Prodi, L.; Stoddart, J. F.; Williams, D. J. *J. Am. Chem. Soc.* **1997**, *119*, 10641−10651.

(11) The papers listed in ref 10 describe systems that can undergo acid−base driven threading/dethreading of amines from crown ethers and can be viewed, therefore, as chemically driven machines.

(12) Preliminary communication on part of this research: Martínez-Díaz, M.-V.; Spencer, N.; Stoddart, J. F. *Angew. Chem., Int. Ed. Engl.* **1997**, *36*, 1904−1907.

(13) Full experimental procedures for all synthetic steps can be found in the Supporting Information.

Scheme 1. Synthetic Protocol Employed To Prepare **1a**-H·3PF_6 and **1b**-H·3PF_6 (X = Cl for **2a**-H·PF_6 and Br for **2b**-H·PF_6)[a]

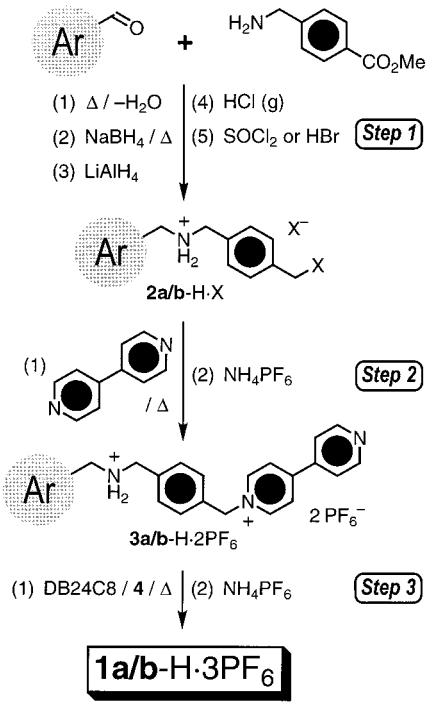

[a] Yields (%) for compounds in **a** series [**b** series]: *Step 1*, 84 [60]; *Step 2*, 66 [25]; *Step 3*, 38 [30].

dorotaxanes with NH_2^+-containing salts, the [2]rotaxanes **1a**-H^{3+} and **1b**-H^{3+} seemed to be appropriate targets for switchable compounds. They were prepared using an approach that relies[15]-on the initial solution-phase formation of pseudorotaxanes between DB24C8 and rodlike components (which already contain an NH_2^+ center and one of the stoppers that prevents macroring loss in the final [2]rotaxanes) followed by stoppering reactions that lead to simultaneous $Bpym^{2+}$/dumbbell formation.

The rotaxanes' rodlike precursors—viz., **3a**-H·2PF_6 and **3b**-H·2PF_6—were prepared by using the route shown in Scheme 1. Since these compounds are only partially soluble in $CHCl_3$ (an ideal solvent for studying hydrogen bonding interactions[10b]), the binding constants (K_a) of their DB24C8 complexes were measured by ^1H NMR spectroscopy in $CDCl_3$–CD_3CN mixtures. By applying the single-point method,[10b] similar K_a values (ca. 2300 M^{-1}) were calculated for the 1:1 complexes [DB24C8·**3a**-H][PF_6]$_2$ and [DB24C8·**3b**-H][PF_6]$_2$ in $CDCl_3$–CD_3CN (1:1).[16] These relatively strong binding constants allowed the production of the [2]rotaxanes in reasonable yields when the appropriate precursors were reacted with 3,5-di-*tert*-butylbenzyl bromide (**4**) in the presence of an excess of DB24C8. The synthesis of **1b**-H·3PF_6 was also performed by an alternative route, specifically, via reaction of **2b**-H·PF_6 with **5**·PF_6 in the presence of DB24C8. Both of the [2]rotaxanes prepared survive chromatography, indicating that both the Anth and 3,5-di-*tert*-butylphenyl (Dtbp) stoppers are large enough to ensure macroring–dumbbell interlocking. The free dumbbell-shaped compounds **6a**-H·3PF_6 and **6b**-H·3PF_6 were prepared by reacting either **3a**-H·2PF_6 or **3b**-H·2PF_6 with **4** in the absence of DB24C8.

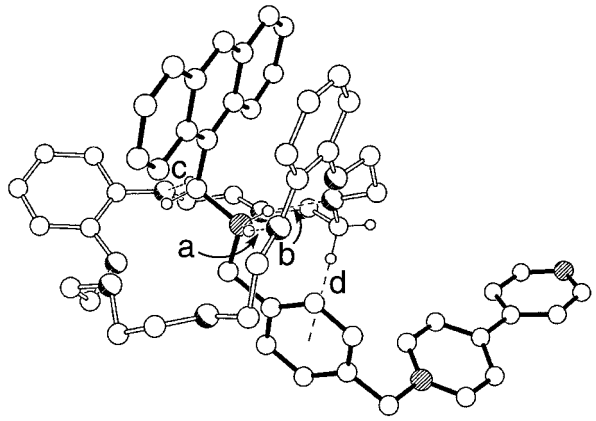

Figure 2. The solid-state superstructure of the [2]pseudorotaxane [DB24C8·**3b**-H]$^{2+}$. Hydrogen bonding distances and angles {[X···O], [H···O] distances (Å), [X–H···O] angles (deg)}: (a) 3.03, 2.14, 166; (b) 3.03, 2.14, 164; (c) 3.28, 2.36, 161. [C–H···π] interaction: (d) [H···π] 2.85 Å, [H···π] vector inclined by 74° to the *p*-Xy ring plane.

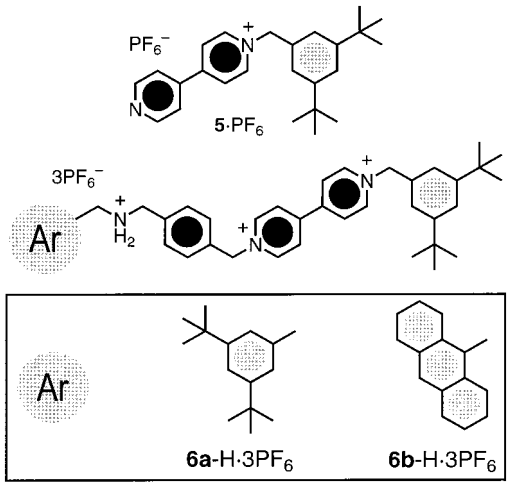

X-ray Crystallography. The X-ray analysis of [DB24C8·**3b**-H][PF_6]$_2$ shows the dication to be threaded through DB24C8's center to generate (Figure 2) a pseudorotaxane with a very similar[10b] geometry to that of closely related complexes. The Anth–$CH_2NH_2^+CH_2$–*p*-Xy (*p*-Xy = *p*-xylyl) portion of the backbone adopts a near planar, all-anti geometry with mean torsional twists about the C–Anth and C–*p*-Xy bonds of 85 and 14°, respectively. The pyridinium (Pym^+) ring is aligned almost orthogonally with the *p*-Xy ring, the associated C–C and C–N^+ torsional angles being 82 and 21°, respectively. The twist angle about the bond linking the pyridyl and Pym^+ rings is ca. 27°. The DB24C8 macrocycle adopts a V-shaped conformation, its two catechol rings being inclined by ca. 79° to each other. Complexation is achieved by [N^+–H···O] and [C–H···O] hydrogen bonds, as well as by [C–H···π] and π–π stacking interactions that occur between the dication's Anth unit and the DB24C8 catechol ring positioned over its center (mean interplanar separation 3.43 Å, centroid···centroid distance 3.63 Å, ring systems inclined by ca. 6°).

An inspection of the packing of the [2]pseudorotaxanes reveals (Figure 3) the presence of helical π–π stacked chains of 1:1 complexes, the Pym^+ ring of one complex being stacked with the Anth unit of its 2_1 screw-related neighbor. The Pym^+ ring of one dication is inclined by ca. 7° to the Anth plane of

(14) Ashton, P. R.; Glink, P. T.; Martínez-Díaz, M.-V.; Stoddart, J. F.; White, A. J. P.; Williams, D. J. *Angew. Chem., Int. Ed. Engl.* **1996**, *35*, 1930–1933.

(15) Ashton, P. R.; Glink, P. T.; Stoddart, J. F.; Tasker, P. A.; White, A. J. P.; Williams, D. J. *Chem. Eur. J.* **1996**, *2*, 729–736.

(16) A K_a of 5120 M^{-1} was calculated for the complex [DB24C8·**2a**-H][PF_6] in $CDCl_3$–CD_3CN (4:1) by the same method.

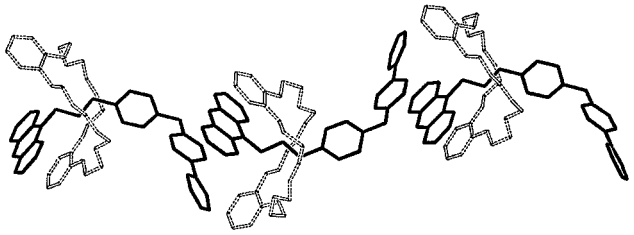

Figure 3. A segment of the π-stacked helical chains {[DB24C8·**3b**-H]$^{2+}$}$_n$.

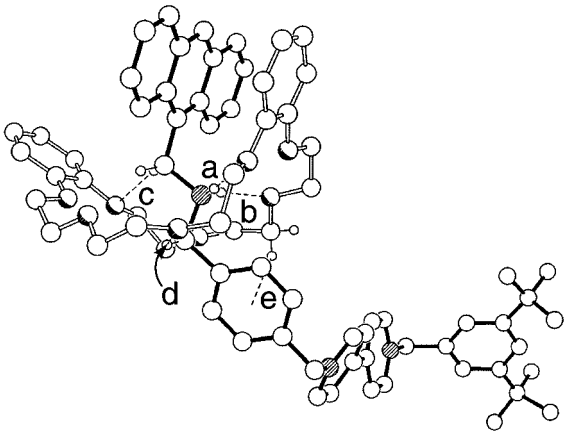

Figure 4. The crystal structure of [2]rotaxane **1b**-H^{3+}. Hydrogen bonding distances and angles with values for the second independent molecule in square brackets {[X···O], [H···O] distances (Å), [X−H···O] angles (deg)}: (a) 3.05, 2.16, 171 [3.12, 2.25, 163]; (b) 3.04, 2.15, 169 [3.09, 2.21, 165]; (c) 3.41, 2.50, 158 [3.22, 2.49, 133]; (d) 3.08, 2.35, 132 [3.36, 2.47, 156]. In the second independent molecule, the [C−H···O] hydrogen bond (d) is formed to the polyether linkage's third oxygen atom, rather than to the second as shown. [C−H···π] interaction (e) [H···π] 2.85 Å [3.10 Å], [H···π] vectors inclined by 81° [77°] to the *p*-Xy ring plane.

the next and overlays two of this unit's rings with centroid··· centroid distances (to the central and outer rings, respectively) of 3.88 and 3.79 Å and a mean interplanar separation of 3.58 Å.

The solid-state structure of **1b**·H·3PF$_6$ reveals (Figure 4) that the addition of the Dtbp stopper, to create the [2]rotaxane, produces little change in the remainder of the system's geometry. The structure contains two crystallographically independent [2]-rotaxane molecules in the asymmetric unit, but with only slight geometrical differences (the parameters of the second independent molecule are given in square brackets). The geometry of the Anth−CH$_2$NH$_2^+$CH$_2$−*p*-Xy portion of the backbone is once again all-anti with the Anth unit oriented approximately orthogonally (ca. 78° [86°]); the *p*-Xy ring is much less steeply inclined with C−*p*-Xy torsional angles of 31° [41°]. The *p*-Xy and nearby Pym$^+$ rings adopt an "open-book" conformation, the torsion angles about the adjoining C−C and C−N$^+$ bonds being 76 and 72° [74 and 64°], respectively. The mean torsional twist around the bond linking the two Pym$^+$ rings is 30° [26°]. The Dtbp terminus assumes a skewed geometry with respect to the proximal Pym$^+$ ring, the respective torsion angles about the connecting N$^+$−C and C−C bonds being 90 and 51° [89 and 79°]. The DB24C8 macroring has a V-shaped conformation, the planes of the catechol rings being inclined by 69° [60°], in a slightly more closed geometry than that observed for the [2]-pseudorotaxane [DB24C8·**3b**-H]$^{2+}$. The [2]rotaxane molecules are stabilized by the same combination of [N$^+$−H···O], [C−H···O] hydrogen bonds and [C−H···π] interactions, as well as

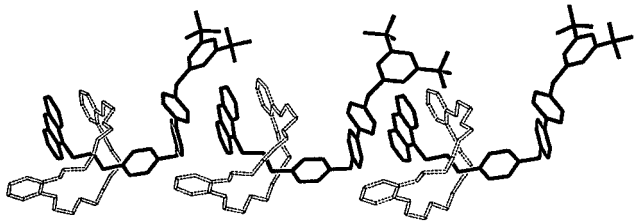

Figure 5. Part of the π-stacked supramolecular array composed of pairs of independent lattice-translated **1b**-H^{3+} molecules.

by $\pi-\pi$ stacking interactions between one of DB24C8's catechol rings and one of the trication's Anth rings.[17]

The packing (Figure 5) of the [2]rotaxanes is similar to that observed for the [2]pseudorotaxane [DB24C8·**3b**-H]$^{2+}$. In **1b**-H·3PF$_6$, however, one of the Pym$^+$ rings of one independent molecule overlays the Anth ring of another, a pattern that is then repeated for lattice-translated crystallographically independent pairs of molecules.[18]

The crystal data, data collection, and refinement parameters for the structures are given in Table 1.

NMR/Mass Spectra. The ^{1}H NMR spectrum of **1a**-H·3PF$_6$ is consistent (Figure 6a) with [2]rotaxane formation. Its data, along with the data for the noninterlocked dumbbell **6a**-H·3PF$_6$, are listed in Table 2. The spectrum demonstrates that DB24C8 binds selectively with the NH$_2^+$ center, since the characteristic[10b] resonance for the four CH$_2$ protons adjacent to a "bound" NH$_2^+$ center, at δ 4.85−4.87, is observable and experiences a downfield shift of ca. 0.2 ppm with respect to the complex formed between DB24C8 and **6a**-H·3PF$_6$. This selective binding was also confirmed by ^{1}H NMR 1D-NOE doubled-pulsed field-gradient spin−echo experiments (GOESY).[19] Selective irradiation of the protons C showed that intercomponent NOEs were detected (Figure 6b) with OCH$_2$ protons on only one of the crown ether's two heterotopic faces. The same effect was noted when the protons A were irradiated selectively. Additionally, we would expect to see another set of signals for a second translational isomer if the DB24C8 macroring were to reside anywhere else, other than on the NH$_2^+$ center, as the movement of the crown ether over the thread's benzenoid units is anticipated[10b] to be slow on the ^{1}H NMR time scale. Since no new sets of resonances, for any additional species, could be detected in the low temperature ^{1}H NMR spectrum (400 MHz, CD$_3$COCD$_3$, 193 K), it was concluded that the DB24C8 macroring is bound to the NH$_2^+$ center with at least 98% selectivity from 193 to 304 K. A detailed analysis of the chemical shift differences experienced by protons C and D indicates that the crown ether's catechol rings are probably, to some extent, sandwiching the *p*-Xy spacer so as to benefit from supplementary stabilization by means of weak $\pi-\pi$ stacking interactions.

The ^{1}H NMR spectrum of the [2]rotaxane **1b**-H·3PF$_6$ shows that the dumbbell and ring components are present in equimolar

(17) The catechol ring is positioned over the central ring of the Anth unit; it is inclined by only ca. 2° [2°], with a ring centroid···ring centroid distance of 3.60 Å [3.50 Å] and a mean interplanar separation of 3.42 Å [3.37 Å].

(18) In one of the two independent $\pi-\pi$ stacking interactions, the Pym$^+$ ring is positioned more above the Anth unit's central ring with an interplanar separation of 3.60 Å and centroid···centroid distances (to the central and outer rings, respectively) of 3.69 and 4.08 Å, the Pym$^+$ and Anth rings being inclined by ca. 12°. For the other $\pi-\pi$ stacking interaction, the interacting Pym$^+$ ring is inclined by 8° and is centered more toward one of the Anth unit's outer rings. The associated ring centroid···ring centroid separations are 3.67 (to the outer ring) and 3.83 Å (to the central ring), the mean interplanar separation being 3.44 Å.

(19) Stonehouse, J.; Adell, P.; Keeler, J.; Shaka, A. J. *J. Am. Chem. Soc.* **1994**, *116*, 6037−6038.

Table 1. Crystal Data, Data Collection, and Refinement Parameters[a]

	[DB24C8·**3b**-H][PF$_6$]$_2$	**1b**-H·3PF$_6$
formula	$C_{57}H_{61}N_3O_8$·2PF$_6$	$C_{72}H_{84}N_3O_8$·3PF$_6$
solvent	MeCN	4Me$_2$CO
formula weight	1247.1	1786.6
color, habit	yellow needles	orange/red rhombs
crystal size (mm)	0.50 × 0.13 × 0.12	0.73 × 0.70 × 0.53
lattice type	monoclinic	triclinic
space group symbol, no.	$P2_1/c$, 14	$P\bar{1}$, 2
cell dimensions		
a (Å)	11.551(1)	20.138(3)
b (Å)	26.371(1)	21.696(5)
c (Å)	18.911(1)	23.916(4)
α (deg)		115.28(2)
β (deg)	97.31(1)	101.73(2)
γ (deg)		97.52(2)
V (Å^3)	5713.8(5)	8967(3)
Z	4	4[b]
D_c (g cm^{-3})	1.450	1.323
F(000)	2592	3744
μ (mm^{-1})	1.56	1.45
θ range (deg)	2.9−60.0	2.1−57.5
no. of unique reflcns		
measd	8387	21069
obsd, $\|F_o\| > 4\sigma(\|F_o\|)$	5771	12294
no. of variables	768	2094
R_1[c]	0.105	0.101
wR_2[d]	0.263	0.252
weighting factors a, b[e]	0.217, 1.242	0.164, 25.900
largest diff peak, hole (eÅ^{-3})	0.57, −0.70	0.85, −0.67

[a] Details in common: graphite monochromated Cu Kα radiation, ω-scans, Siemens P4/RA diffractometer, 203 K, refinement based on F^2. [b] There are two crystallographically independent molecules in the asymmetric unit. [c] $R_1 = \sum||F_o| - |F_c||/\sum|F_o|$. [d] $wR_2 = \{\sum[w(F_o^2 - F_c^2)^2]/\sum[w(F_o^2)^2]\}^{1/2}$. [e] $w^{-1} = \sigma^2(F_o^2) + (aP)^2 + bP$.

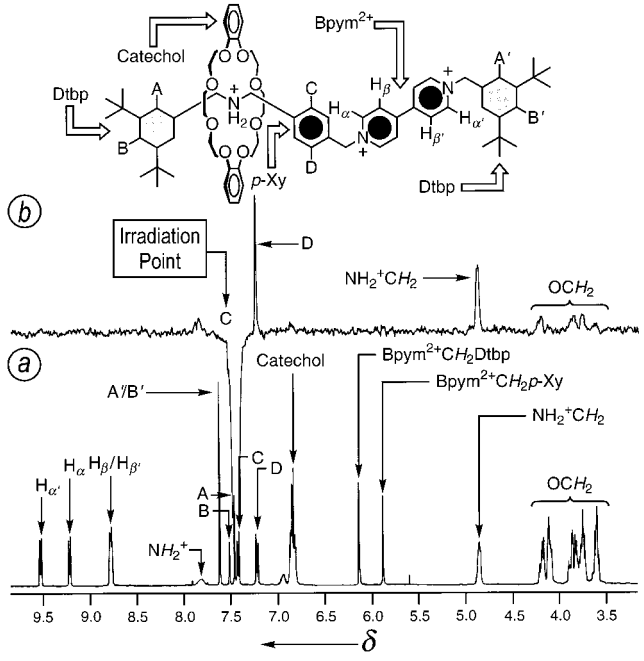

Figure 6. (a) ^{1}H NMR spectrum (400 MHz, CD_3COCD_3, 304 K) of **1a**-H·3PF$_6$ and (b) the GOESY spectrum following irradiation of the protons C.

amounts and are also interlocked with one another. The DB24C8 macrocycle binds selectively with the NH_2^+ center, the characteristic resonances for the four CH_2 protons adjacent to this binding site experiencing a downfield shift of ca. 0.5 ppm upon rotaxane formation. As signals are observed only for

Table 2. ^{1}H NMR Data (400 MHz, CD_3COCD_3, 304 K)[a,b]

	1a-H·3PF$_6$	**1a**·2PF$_6$	**6a**-H·3PF$_6$	**6a**·2PF$_6$
$H_{\alpha'}$	9.56	9.44	9.53	9.49 (br)
H_α	9.23	9.29	9.42	9.49 (br)
$H_{\beta'}$	8.79−8.80	8.96	8.78	8.78 (br)
H_β	8.79−8.80	8.77	8.76	8.78 (br)
A′	7.61	7.63	7.61	7.61
B′	7.61	7.63	7.61	7.61
A	7.46	7.22	7.43	7.22
B	7.51	7.34	7.56	7.34
C	7.41	7.37	7.74	7.61
D	7.21	7.37	7.70	7.52
Bpym^{2+}−CH_2−Dtbp	6.14	5.96	6.20	6.13 (br)
Bpym^{2+}−CH_2−*p*-Xy	5.88	5.79	6.14	6.13 (br)
NH_2^+−CH_2−Dtbp	4.85−4.87	3.73	4.70	3.82
NH_2^+−CH_2−*p*-Xy	4.85−4.87	3.73	4.63	3.75
C(CH_3)$_3$	1.23, 1.30	1.30, 1.33	1.28, 1.30	1.30, 1.31
catechol	6.83−6.86	6.74−6.81		
OCH_2	3.58−4.22	3.09−4.04		

[a] The proton descriptors are explained in Figure 6. [b] All chemical shift values are reported on the δ scale.

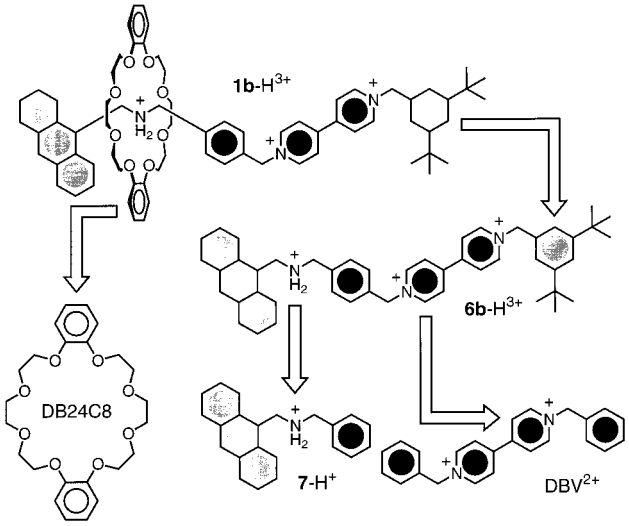

Figure 7. Logical progression from [2]rotaxane **1b**-H^{3+}, through its constituents, to model compounds for the chromophoric and redox-active units of dumbbell **6b**-H^{3+}.

the complexed NH_2^+ ion, it may be presumed that the crown ether resides exclusively on this site, at least on the NMR time scale.

LSI mass spectroscopy also provides evidence for the formation of the [2]rotaxanes. Base peaks were observed, at m/z 1420 and 1408, corresponding to the species [**1a**-H·2PF$_6$]$^+$ and [**1b**-H·2PF$_6$]$^+$.

Photophysical, Photochemical, and Electrochemical Properties. The photophysical, photochemical and electrochemical investigations have been performed on **1b**-H^{3+} because it possesses an additional chromophoric and electroactive unit—namely, the Anth stopper—in comparison to **1a**-H^{3+}. To elucidate the behavior of a multicomponent species, reference has to be made to the properties of its molecular components and of suitable model compounds for the single chromophoric and electroactive units. Suitable model compounds for the Anth-bearing NH_2^+ center and Bpym^{2+} unit of the dumbbell **6b**-H^{3+} are (Figure 7) the 9-(benzylammoniummethyl)anthracene cation (**7**-H$^+$) and the dibenzylviologen dication (DBV^{2+}), respectively.

(a) Absorption and Emission Spectra. Figure 8 shows the absorption spectra of the dumbbell component **6b**-H^{3+} and the model compounds, viz., **7**-H$^+$ and DBV^{2+}, for its chromophoric

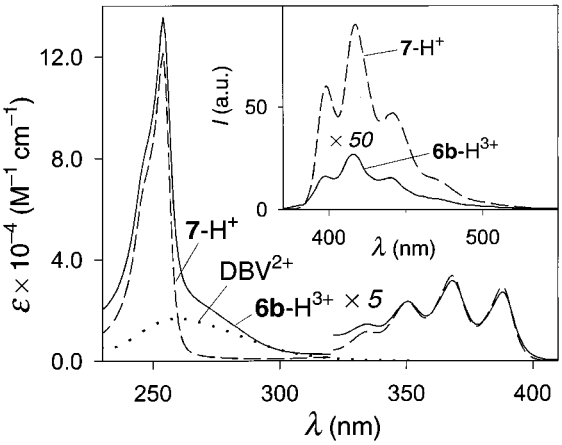

Figure 8. Absorption spectra (MeCN, 293 K) for **6b**-H^{3+} (solid line) and its chromophoric units, viz., **7**-H^+ (dashed line) and DBV^{2+} (dotted line). Inset: fluorescence spectra of **6b**-H^{3+} and **7**-H^+ upon excitation in the low energy Anth band.

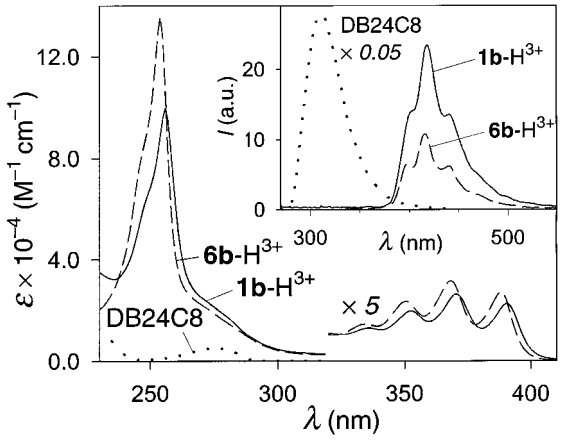

Figure 9. Absorption and (inset) fluorescence spectra (MeCN, 293 K) of **1b**-H^{3+} and its components, viz., DB24C8 and **6b**-H^{3+}. Excitation was performed in the low-energy Anth band for both **1b**-H^{3+} and **6b**-H^{3+}, as well as at 277 nm for DB24C8.

Table 3. Fluorescence and Photochemical Data[a]

compd	λ_{max}[b] (nm)	I_{em}[c]	Φ_r[d]
6b-H^{3+}	417	1.0	0.8
1b-H^{3+}	417[e]	2.1	1.0
6b^{2+}	411	0.5	1.8
1b^{2+}	411[e]	1.1	2.6

[a] Air equilibrated MeCN solutions, 293 K. [b] Wavelength of the emission maximum. [c] Relative emission intensity upon excitation in the low-energy anthracene band. In this scale, the relative emission intensity of model compound **7**-H^+ is 170 (corresponding to a quantum yield of 0.3). [d] Relative photoreaction quantum yield upon irradiation at 365 nm. In this scale, the relative photoreaction quantum yield of **7**-H^+ is 12 (corresponding to a quantum yield of 6×10^{-4}). [e] Upon excitation at 277 nm, no emission can be seen in the 310 nm region where DB24C8 exhibits an intense fluorescence.

units. The most intense absorption features, arising from the Anth unit, are essentially unperturbed on going from **7**-H^+ to **6b**-H^{3+}. In particular, it is only the Anth moiety that absorbs in the spectral region above 350 nm, a property that allows us to perform selective excitation of this unit when necessary. The cation **7**-H^+ shows a strong and structured fluorescence band in the visible region that is characteristic[20] of the Anth unit, whereas DBV^{2+} is not emissive. As shown in the inset of Figure 8, such a fluorescence band is still present in **6b**-H^{3+}, but with (Table 3) a 170-fold reduction in intensity. This strong quenching can be assigned to a photoinduced electron transfer from the fluorescent excited state of the Anth moiety to the $Bpym^{2+}$ unit (vide infra).

Figure 9 compares the absorption spectra of **1b**-H^{3+} and its constituents, viz., **6b**-H^{3+} and DB24C8. Both the dominant Anth-based absorption features, i.e., the strong band around 255 nm and the weaker structured band in the 320−400 nm region, are perturbed. As shown in the inset, the intense crown ether fluorescence band of the [2]rotaxane (λ_{max} = 308 nm), assigned[7b,21] to the lowest singlet excited state of the dioxybenzene units, is completely quenched. Conversely, the fluorescence band of the Anth unit, which is strongly quenched in **6b**-H^{3+} (vide supra), partially regains (Table 3) its intensity. The quenching of the crown ether's fluorescent dioxybenzene excited state (energy ca. 4 eV) can be ascribed to energy transfer to the nearby Anth moiety, as previously observed[10c] in a related system, and/or to strongly exoergonic electron transfer to the $Bpym^{2+}$ unit.[21] The fluorescent behavior of the Anth-based unit will be discussed more fully in the section dealing with the switching processes.

(b) Photochemical Behavior. It is well-known[22] that the triplet excited state of Anth derivatives sensitizes the formation of singlet oxygen ($^1\Delta)O_2$ in aerated solutions. This species reacts with the central Anth ring to provide an 1,10-endoperoxide that then evolves toward other products. Such a photoreaction, which can be followed easily by the disappearance of the characteristic Anth-type absorption and fluorescence bands, is moderately efficient in the case of **7**-H^+. However, it is much less efficient (Table 3) for both **6b**-H^{3+} and **1b**-H^{3+}. This strong photoreactivity decrease can be attributed to the quenching of the Anth moiety's singlet excited state by the $Bpym^{2+}$ unit, preventing formation of the Anth triplet excited state.

(c) Electrochemical Behavior. The data for the electrochemical experiments are listed in Table 4. All the reduction processes are fully reversible, while the oxidation processes are not. Figure 10 shows a correlation of the potential values obtained for **1b**-H^{3+}, its components, viz., **6b**-H^{3+} and DB24C8, and three reference complexes. The dumbbell **6b**-H^{3+} exhibits three monoelectronic reduction processes and one oxidation process. This behavior is exactly that predicted from the electrochemical properties associated with the electroactive units of the model compounds DBV^{2+} and **7**-H^+. The [2]rotaxane **1b**-H^{3+} shows three reduction processes that, by comparison with the behavior of **6b**-H^{3+}, can be assigned straightforwardly to the first and second one-electron reductions of the $Bpym^{2+}$ unit and to the one-electron reduction of the Anth unit. The fact that the reduction of the $Bpym^{2+}$ unit takes place at the same potentials in **6b**-H^{3+} and **1b**-H^{3+} provides further evidence that the DB24C8 macroring is located on the dumbbell's NH_2^+ station. On oxidation, **1b**-H^{3+} shows two processes whose assignment is less simple. From the behavior of its separate dumbbell and macroring components, three oxidation processes would, in fact, be expected—one localized on the Anth unit and two on the crown ether. Since the crown ether's oxidation processes are likely to be affected by the NH_2^+ ion within its

(20) Berlman, I. B. *Handbook of Fluorescence Spectra of Aromatic Compounds*; Academic: London, 1965.

(21) Anelli, P.-L.; Ashton, P. R.; Ballardini, R.; Balzani, V.; Delgado, M.; Gandolfi, M. T.; Goodnow, T. T.; Kaifer, A. E.; Philp, D.; Pietraszkiewicz, M.; Prodi, L.; Reddington, M. V.; Slawin, A. M. Z.; Spencer, N.; Stoddart, J. F.; Vicent, C.; Williams, D. J. *J. Am. Chem. Soc*. **1992**, *114*, 193−218.

(22) Turro, N. J. *Modern Molecular Photochemistry*; Benjamin: Menlo Park, CA, 1978.

Table 4. Electrochemical Data[a]

compd	reduction	oxidation[b]
DB24C8		+1.32, +1.47
c		+1.32, +1.47
d		+1.31, +1.45
DBV^{2+}	−0.37, −0.79	
c	−0.37, −0.79	
d	−0.37, −0.79	
7-H^+	−1.98	+1.43
7	−1.98	+1.09,[e] +1.43[f]
7-H^+ [d]	−1.99	+1.41
6b-H^{3+}	−0.35,[g] −0.78,[g] −1.98[f]	+1.43
6b^{2+}	−0.36,[g] −0.78,[g] −1.98[f]	+1.09,[e] +1.43[f]
6b-H^{3+} [d]	−0.35,[g] −0.78,[g] −1.98[f]	+1.41
1b-H^{3+}	−0.35,[g] −0.77,[g] −2.02[f]	+1.39,[f] +1.47[h,i]
1b^{2+}	−0.59,[g,j] −0.77,[g] −2.03[f]	+1.12,[e] +1.39,[f] +1.50[h,i]
1b-H^{3+} [d]	−0.35,[g] −0.78,[g] −2.02[f]	+1.38,[f] +1.47[h,i]

[a] Ar-purged MeCN solutions, 293 K; halfwave potential values in V vs SCE; reversible and monoelectronic processes, unless noted otherwise. [b] All oxidation processes are not fully reversible—potential values estimated from DPV peaks. [c] After addition of 1 equiv of Bu_3N. [d] After addition of 1 equiv of Bu_3N and subsequent treatment with 1 equiv of TfOH. [e] NH_2^+ unit. [f] Anth unit. [g] $Bpym^{2+}$ unit. [h] Crown ether. [i] More than one electron is involved. [j] Value obtained by simulation. See text for details.

cavity, we have examined[23] the electrochemical behavior of the [2]pseudorotaxane model[10b] $[DB24C8\cdot DBA]^+$. This complex displays only one oxidation process, at +1.46 V, which, as foreseen, is displaced toward more positive potentials with respect to the first oxidation process of DB24C8. This irreversible process seems to involve more than one electron and can be assigned to the simultaneous oxidation of the crown ether's noninteracting dioxybenzene units. An alternative possibility is that the second one-electron oxidation of the crown ether occurs at the potential of the first because the first oxidation process causes the displacement of the positively charged macroring away from the NH_2^+ center. In any case, the oxidation behavior of [2]pseudorotaxane $[DB24C8\cdot DBA]^+$ allows us to assign the first and second oxidation processes of the [2]rotaxane **1b**-H^{3+} to the Anth and crown ether units, respectively.

The [2]Rotaxanes' Switching Processes. We have already established that the [2]rotaxanes' DB24C8 component resides exclusively on the NH_2^+ recognition center. Bases that can deprotonate this center could act as chemical inputs that promote (Figure 1) the movement of the crown ether to the $Bpym^{2+}$ unit. The choice of base to be used was not easy, since the dumbbell's $Bpym^{2+}$ unit is very sensitive to nucleophilic bases. It was found that diisopropylethylamine[12] (*i*-Pr_2NEt) and tributylamine (Bu_3N) are ideal bases to drive the switching process because they are strong enough to deprotonate the NH_2^+ center while behaving concurrently as very weak (i.e., unreactive) nucleophiles toward $Bpym^{2+}$ units. Reprotonation can be performed by the addition of a suitable acid (e.g., trifluoroacetic (CF_3CO_2H) or triflic (TfOH) acids). The acid−base switching processes have been monitored by ^1H NMR spectroscopy for both [2]-rotaxanes. The switching process has also been investigated by photophysical and electrochemical techniques for **1b**-H^{3+}.

(a) ^1H NMR Experiments. A slight molar excess of *i*-Pr_2NEt or Bu_3N was added to a solution of **1a**-H·$3PF_6$ (ca. 4.7 mM) in CD_3COCD_3. Immediately, the solution's appearance changed from clear to yellow, indicating[24] the creation of CT interactions between DB24C8's catechol rings and the $Bpym^{2+}$ dication. The ^1H NMR spectrum shows (Figure 11) that, on base addition, deprotonation of the NH_2^+ center occurs, while leaving the $Bpym^{2+}$ unit intact. Resonances for the CH_2-$NH_2^+CH_2$ protons disappear and new signals, which can be assigned to CH_2NHCH_2 protons, become visible. Moreover, the ^1H NMR spectrum of **1a**·$2PF_6$ shows dramatic chemical shift changes compared to that of **1a**-H·$3PF_6$, especially (Table 2) for the resonances associated with the $Bpym^{2+}$ and *p*-Xy protons, a feature that suggests that the DB24C8 macroring interacts asymmetrically with the $Bpym^{2+}$ unit.

^1H NMR studies on the deprotonated [2]rotaxane **1a**·$2PF_6$ (400 MHz, CD_3COCD_3, 193 to 304 K) reveal that the DB24C8 macroring resides *exclusively* on the $Bpym^{2+}$ recognition site. Although the spectrum broadens below 233 K, no supplementary sets of resonances, for any other translational isomers, are evident. Upon addition of CF_3CO_2H, the $NH_2^+CH_2$ protons resonate at δ 4.85−4.87, suggesting that the DB24C8 component shuttles back completely to the NH_2^+ recognition site following reprotonation. In other words, the [2]rotaxane **1a**-H·$3PF_6$ exhibits fully reversible switching (Figure 1) of its crown ether macroring between the dumbbell's two stations via de-/reprotonation.

The Anth-containing [2]rotaxane **1b**-H·$3PF_6$ behaves similarly, as deprotonation of the NH_2^+ center occurs when a slight molar excess of *i*-Pr_2NEt is added to a CD_3COCD_3 solution of **1b**-H·$3PF_6$. The resonances (δ 5.45 and 5.73) for the four CH_2-$NH_2^+CH_2$ protons disappear and new resonances, at δ 4.00 and 4.70, become visible for the CH_2NHCH_2 moieties. Furthermore, the macrocycle moves to interact with the $Bpym^{2+}$ unit, resulting in changes to the α- and β-$Bpym^{2+}$ protons' resonances (δ [$\Delta\delta$] values for $H_{\alpha'}$, H_α, $H_{\beta'}$, and H_β (ppm): 9.42 [−0.12], 9.31 [+0.05], 8.94 [+0.19], and 8.74 [−0.01]). On addition of CF_3-CO_2H, the original ^1H NMR spectrum is regenerated, demonstrating, once again, that the switching process is reversible.

(b) Absorption and Emission Experiments. Addition of 1 equiv of Bu_3N to MeCN solutions of the [2]rotaxane **1b**-H^{3+}, dumbbell **6b**-H^{3+}, or model compound **7**-H^+ furnishes their deprotonated forms. In the case of **6b**-H^{3+} and **7**-H^+, deprotonation effects only very small changes in the Anth-based structured band (300−400 nm). Similarly, the stronger band, centered at ca. 255 nm, shows only a small intensity decrease. Indeed, this is the behavior expected[20] for a small change in the nature of an 9-Anth substituent. For **1b**-H^{3+}, deprotonation is accompanied by a small blue shift and an increase in the absorbance of both the high (Figure 12a) and low energy Anth-based bands. This behavior indicates[20] a change in the perturbation of the Anth chromophoric group along both of its symmetry axes and is consistent with the displacement of DB24C8's aromatic moieties from the Anth unit. Even from a purely empirical viewpoint, it can be noticed that, upon deprotonation, the intensity of the Anth absorption bands *decreases* for **6b**-H^{3+}, while it *increases* for **1b**-H^{3+}. Consequently, the spectral changes observed upon deprotonation of **1b**-H^{3+} cannot be due simply to proton removal from the NH_2^+ center—they must be assigned to a change in the interaction between the Anth unit and DB24C8. As the macroring situated on the NH_2^+ recognition site affects the Anth bands (Figure 9), accompanied by the fact that the deprotonated (**6b**$^{2+}$ and **1b**$^{2+}$) species exhibit very similar absorption spectra, we can conclude

(23) The electrochemical experiments were performed on an Ar-purged MeCN solution containing 1.2×10^{-3} M DB24C8 and 5.0×10^{-2} M DBA·PF_6. Under these conditions, DB24C8 is complexed almost quantitatively by DBA^+ to generate the [2]pseudorotaxane $[DB24C8\cdot DBA]^+$.

(24) Ashton, P. R.; Langford, S. J.; Spencer, N.; Stoddart, J. F.; White, A. J. P.; Williams, D. J. *Chem. Commun.* **1996**, 1387−1388.

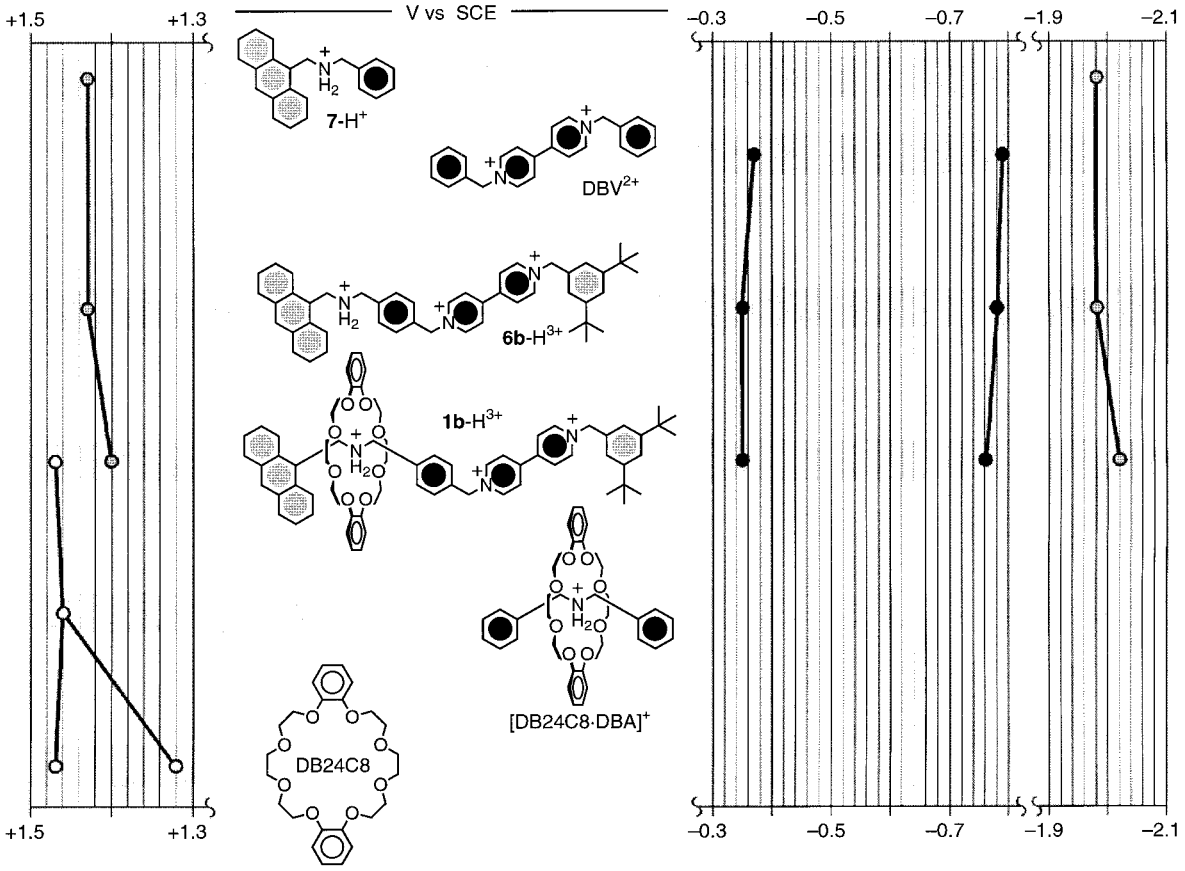

Figure 10. Correlation of the potentials (V vs SCE) for the oxidation/reduction processes of **1b**-H^{3+}, its constituents (**6b**-H^{3+} and DB24C8), and some model compounds/complexes.

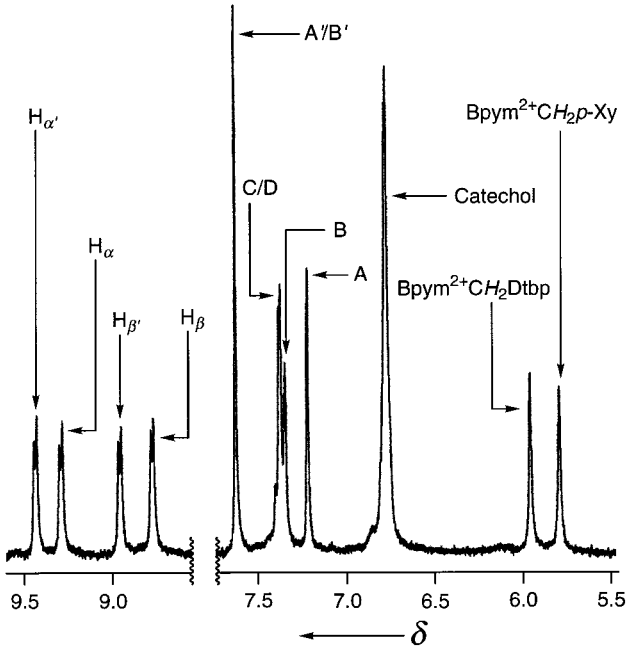

Figure 11. Partial ^{1}H NMR spectrum (400 MHz, CD_3COCD_3, 304 K) of **1a**·$2PF_6$. The proton descriptors are defined in Figure 6.

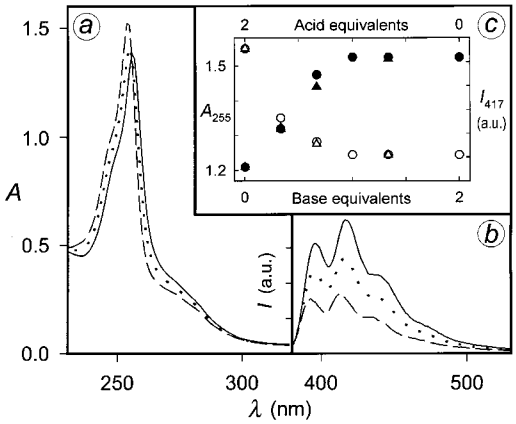

Figure 12. Spectral changes (MeCN, 293 K) for **1b**-H^{3+} on addition of Bu_3N: (a) Anth-based high-energy absorption band; (b) Anth-based fluorescence (excitation at the isosbestic point (353 nm)). The solid, dotted, and dashed lines refer, respectively, to [Bu_3N]/[**1b**-H^{3+}] ratios of 0, 0.5, and 1. Inset (c) shows the titration curves for absorbance at 255 nm (●) and emission intensity at 417 nm (○). The changes can be reversed completely by addition of TfOH (absorbance (▲) and emission intensity (△)).

that deprotonation of the NH_2^+ site of **1b**-H^{3+} drives the crown ether away from the Anth moiety.

Deprotonation also produces (Figure 12b) an intensity decrease for the Anth emission bands of both **6b**-H^{3+} (and its model compound **7**-H^+) and **1b**-H^{3+}. For **1b**-H^{3+}, both the changes caused by deprotonation, viz., in the absorbance at 255 nm and in the emission intensity at 417 nm, reach a plateau after addition of 1 equiv of base (Bu_3N), and can be completely reversed (Figure 12c) by addition of a stoichiometric amount of TfOH.

The Anth's fluorescence quenching processes, which can occur in the protonated/deprotonated species, are depicted schematically in Figure 13. Intermolecular quenching processes can be neglected, since the lifetime of the excited Anth unit is very short (8.0 ns for model compound **7**-H^+) and the solutions used are very dilute (2×10^{-5} M). The energy of the Anth

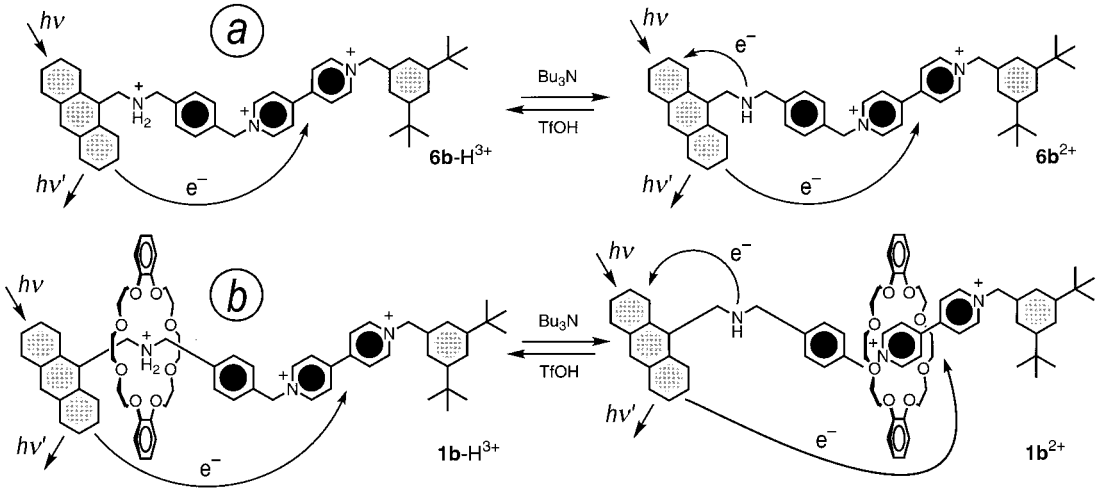

Figure 13. Photoinduced processes in the (a) dumbbell components **6b**-H^{3+}/**6b**$^{2+}$ and (b) [2]rotaxanes **1b**-H^{3+}/**1b**$^{2+}$ that involve the Anth chromophoric group.

moiety's fluorescent excited state is ca. 3.3 eV, the potentials for the oxidation and reduction processes of the Anth unit in **6b**-H^{3+} (and also in **7**-H^{+}) being +1.43 and −1.98 V vs SCE, respectively. Hence, the intensity decrease (Table 3) for the Anth emission band of **6b**-H^{3+}, with respect to **7**-H^{+}, can be ascribed to oxidative quenching of the fluorescent excited state by the Bpym^{2+} unit (reduction potential −0.35 V). The further decrease observed upon deprotonation of **6b**-H^{3+} can be attributed to the slightly exoergonic reductive quenching of the Anth fluorescent excited state by the newly created amino group (which is oxidized at +1.09 V). The emission intensity increase on going from **6b**-H^{3+} to **1b**-H^{3+} can be credited to the interposition of the crown ether macroring between the Anth moiety and the Bpym^{2+} quencher. The emission intensity decrease upon deprotonation of **1b**-H^{3+} can be attributed to further quenching by the amino group that is generated. Finally, the fact that the emission intensity of **1b**$^{2+}$ is larger than that of **6b**$^{2+}$ can, once again, be considered to arise from the protection offered by DB24C8 toward the interaction between the excited state of the Anth moiety and the Bpym^{2+} quencher.

The deprotonated form of the [2]rotaxane does not show any fluorescence from the DB24C8 component, as is[21,25] the norm for aromatic crown ethers engaged in CT interactions.

(c) Photochemical Experiments. In aerated solutions, both **6b**-H^{3+} and **1b**-H^{3+} undergo a low efficiency photochemical reaction that can be followed (vide supra) through the changes in the absorption and emission spectra. The photoreactions' quantum yields (Table 3) depend on both protonation state and macroring position. However, any interpretation of the data dealing with the switching process is precluded by the large number of possible intervening factors. The photoreaction occurs[22] in the Anth unit's lowest triplet excited state, so that the protonation state and macroring position can now participate at three different levels involving the (1) relative concentration of excited singlets, (2) efficiency of intersystem crossing, and (3) intrinsic triplet reactivity.

(d) Electrochemical Experiments. The electrochemical behavior of deprotonated forms **6b**$^{2+}$ and **1b**$^{2+}$ has been investigated and compared with that of their protonated forms (vide supra). The potential values (Table 4) demonstrate that the processes exhibited by **6b**-H^{3+}, along with those of **7**-H^{+} and DBV^{2+}, are not affected by deprotonation. The only difference between the electrochemical behavior of the dumbbell's protonated/deprotonated forms (and also of **7**-H^{+}) is the presence of a characteristic irreversible process, at ca. +1.1 V vs SCE, resulting from the oxidation of the amine unit formed by the deprotonation of the NH_2^{+} center.

The deprotonated [2]rotaxane **1b**$^{2+}$ displays three separate reduction and oxidation processes. On the reduction side, a comparison between the behavior of **1b**-H^{3+} and **1b**$^{2+}$ shows (Figure 14a) that deprotonation shifts the Bpym^{2+} unit's first reduction process strongly toward more negative potentials. On the other hand, deprotonation does not affect this unit's second reduction or the reduction of the Anth moiety. The displacement of the first reduction process toward more negative potentials indicates,[21] along with the NMR and photophysical results, that the Bpym^{2+} unit is engaged in donor−acceptor interactions in **1b**$^{2+}$, a fact that is consistent with the switching of the DB24C8 macroring from the NH_2^{+} to the Bpym^{2+} recognition site upon deprotonation of **1b**-H^{3+}. It can also be noticed that the first reduction process of **1b**$^{2+}$ is characterized by a very large separation between the cathodic and anodic peaks and by some other features that will be discussed below in greater detail. For the present discussion, it is important to note that the cathodic and anodic peaks move toward more and less negative potentials, respectively, when the scan rate is increased. This trend attests to the fact that reduction is followed by a rearrangement process that occurs on the time scale of the electrochemical experiments. The nature of such a process is elucidated from the characteristics of the Bpym^{2+} unit's second reduction, whose potential value practically coincides with that of the dumbbell component. This property means that the monoreduced Bpym^{2+} unit of **1b**$^{2+}$ is no longer engaged in donor−acceptor interactions, since even the second reduction potential is displaced[21,25] toward more negative values when a Bpym^{2+} unit is forced to remain within a crown ether's cavity. In addition, the complete reversibility of the second reduction process indicates that the system does not undergo any further rearrangements after one-electron reduction. Therefore, the first one-electron reduction process promotes the displacement of DB24C8 back toward the $NHCH_2$−Anth moiety of **1b**$^{2+}$. Furthermore, it is reasonable to expect that oxidation of the crown ether also leads to its displacement from the Bpym^{2+} unit. Unfortunately, the fact that the oxidation process is not

(25) (a) Ashton, P. R.; Ballardini, R.; Balzani, V.; Belohradsky, M.; Gandolfi, M. T.; Philp, D.; Prodi, L.; Raymo, F. M.; Reddington, M. V.; Spencer, N.; Stoddart, J. F.; Venturi, M.; Williams, D. J. *J. Am. Chem. Soc.* **1996**, *118*, 4931−4951. (b) Asakawa, M.; Ashton, P. R.; Ballardini, R.; Balzani, V.; Belohradsky, M.; Gandolfi, M. T.; Kocian, O.; Prodi, L.; Raymo, F. M.; Stoddart, J. F.; Venturi, M. *J. Am. Chem. Soc.* **1997**, *119*, 302−310.

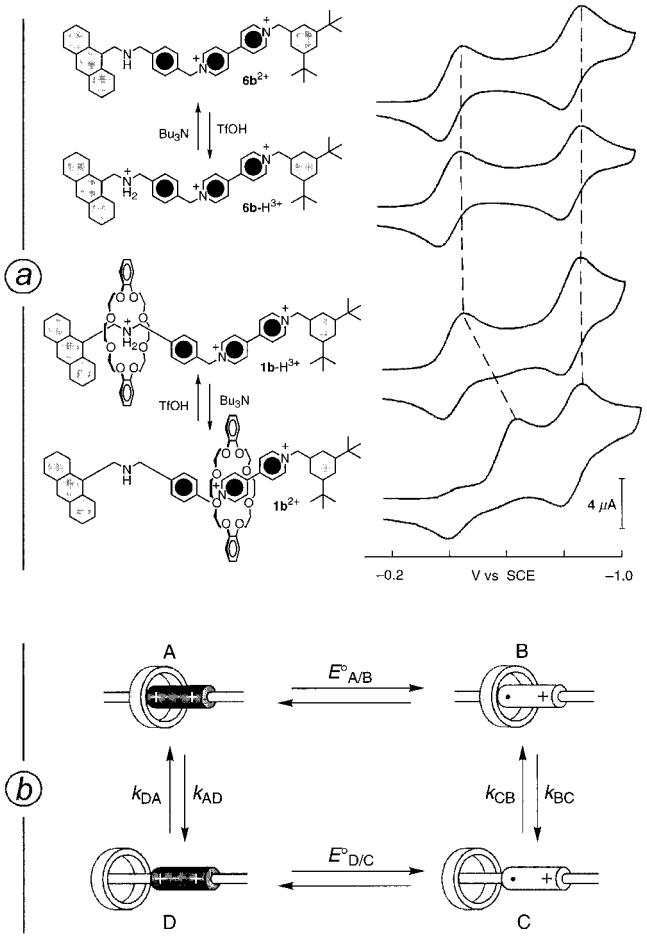

Figure 14. (a) Cyclic voltammetric behavior on reduction of the dumbbell components **6b**$^{2+}$/**6b**-H^{3+} and [2]rotaxanes **1b**-H^{3+}/**1b**$^{2+}$ (Ar-purged MeCN solution, scan rate 50 mV s^{-1}). The current intensity has been corrected to account for differences in diffusion coefficients. (b) Dual-pathway square-scheme mechanism for the **1b**$^{2+/+}$ system. Only the Bpym^{2+} station and macroring are shown (schematically) to represent the mechanical movements involved. Species A and C represent the stable co-conformations of **1b**$^{2+}$ and **1b**$^{+}$, respectively, whereas B and D are metastable intermediates.

completely reversible prevents an investigation of its kinetic implications. Additional evidence that deprotonation of **1b**-H^{3+} promotes the movement of DB24C8 to the Bpym^{2+} unit is obtained by comparing the oxidation behavior of **1b**-H^{3+} and **1b**$^{2+}$. Whereas the Anth unit's oxidation process occurs at the same potential in both rotaxanes, the crown ether's oxidation is shifted toward more positive potentials, by 30 mV, in **1b**$^{2+}$, indicating[21,25] that the DB24C8 macroring becomes engaged in π-donor−π-acceptor interactions after deprotonation.

It will be recalled that the cyclic voltammetric pattern of the first reduction process of **1b**$^{2+}$ is indicative of kinetic complications, a result that is not unexpected for systems in which redox processes can induce mechanical motions.[7] The behavior observed can be discussed on the basis of a square scheme[26] and can be elucidated by experiments performed at different scan rates. On increasing the scan rate from 10 to 1000 mV s^{-1}, the cathodic peak moves toward more negative potentials, reaching a value of −0.62 V, while the anodic peak moves toward less negative potentials, up to −0.30 V. Furthermore, the small oxidation and reduction waves, located at −0.53 and −0.38 V, respectively, tend to disappear as the rate increases. According to the square scheme shown in Figure 14b, the wave at more negative potential is assigned to the redox couple A/B, while that at less negative potential is ascribed to D/C. The results obtained suggest that dethreading of A and rethreading of C and D occur in the time scale of the electrochemical experiment (10−1000 mV s^{-1}), dethreading of monoreduced B occurring at a faster rate. A simple digital simulation of the cyclic voltammetric patterns shows that $E°_{A/B} = -0.59$ V, $E°_{D/C} = -0.34$ V, $k_{AD} \approx 0.15$ s^{-1}, $k_{DA} \leq 2.5$ s^{-1}, $k_{BC} \geq 100$ s^{-1}, and $k_{CB} \approx 1$ s^{-1}.

It can be noticed that the Bpym^{2+} unit's first reduction potential shifts to a much greater extent when it is engaged with DB24C8 in **1b**$^{2+}$ with respect to rotaxanes and catenanes in which a Bpym^{2+} unit undergoes donor−acceptor interactions with crown ethers such as BPP34C10[7b,21,25] and 1,5-dinaphtho[38]crown-10 (1/5DN38C10).[7b,e,25b] Since DB24C8 is a poorer electron donor than both of these crown ethers, the effect cannot be accredited to a stronger donor−acceptor interaction. NMR experiments on solutions of **1b**$^{2+}$ indicate (vide supra) that DB24C8 surrounds predominantly one Pym^{+} ring of the Bpym^{2+} unit on account of its (relatively) small cavity. Such an asymmetric interaction could influence the twist angle between the two Pym^{+} rings, which is known[27] to play a major role in shifting the value of the reduction potential. Structural effects and steric crowding can account for the fact that macroring dethreading from the reduced Bpym^{2+} unit (process B → C) is fast, while rethreading (process D → A) is very slow.

To test the reversibility of the switching process, we have added an equivalent of TfOH to the **1b**$^{2+}$ solution, obtained by deprotonation of **1b**-H^{3+}, before electrochemical analyses. The results obtained match those exhibited by the original **1b**-H^{3+} species exactly, indicating that protonation of the amine group propels the crown ether from the Bpym^{2+} unit back to the regenerated NH_2^+ recognition center, as also evidenced by NMR and photophysical experiments. The switching of the macroring between recognition centers can be repeated by successive acid−base treatments without any electrochemical evidence of side reactions.

Conclusions

The syntheses of two [2]rotaxanes, viz., **1a**-H^{3+} and **1b**-H^{3+}, composed of a DB24C8 macroring bound mechanically to a dumbbell-shaped component endowed with an NH_2^+ center and a Bpym^{2+} unit, have been achieved by using the principles of synthetic supramolecular chemistry.[28] Acid−base switching experiments, monitored by ^{1}H NMR spectroscopy, demonstrated that, upon addition of an appropriate base to a solution of either of the [2]rotaxanes, the crown ether switches from the NH_2^+ to the Bpym^{2+} station. Treatment with acid restores the NH_2^+ center and reverses the process. In the case of anthracene-bearing **1b**-H^{3+}, the reversible switching process has also been monitored completely by means of electrochemical and photophysical techniques. This particular controllable molecular shuttle symbolizes a major performance enhancement over other previously reported switching systems.

Acknowledgment. This research was supported by the Engineering and Physical Sciences Research Council (UK), the University of Bologna (Funds for Selected Research Topics), and the EU (TMR Grant No. FMRX-CT96-0076). We thank

(26) For a recent example, see: Villeneuve, N. M.; Schroeder, R. R.; Ochrymowycz, L. A.; Rorabacher, D. B. *Inorg. Chem.* **1997**, *36*, 4475−4483.

(27) Wardman, P. *J. Phys. Chem. Ref. Data* **1989**, *18*, 1637−1755.

(28) Fyfe, M. C. T.; Stoddart, J. F. *Acc. Chem. Res.* **1997**, *30*, 393−401.

the Ministerio de Educación y Ciencia (Spain) for a Postdoctoral Fellowship to M.-V.M.-D.

Supporting Information Available: Experimental procedures, X-ray crystallographic data, and cyclic voltammetric patterns for $\mathbf{1b}^{2+}$ (40 pages, print/PDF). See any current masthead page for ordering information and Web access instructions.

JA982167M